PNAS
www.pnas.org

Supplementary Information for

GABA-stimulated adipose-derived stem cells suppress subcutaneous adipose inflammation in obesity

Injae Hwang[1], Kyuri Jo[2], Kyung Cheul Shin[1], Jong In Kim[1], Yul Ji[1], Yoon Jeong Park[1,3], Jeu Park[1], Yong Geun Jeon[1], Sojeong Ka[1], Sujin Suk[4], Hye-Lim Noh[4], Sung Sik Choe[1], Assim A. Alfadda[5], Jason K. Kim[4], Sun Kim[2], and Jae Bum Kim[1,3#]

[1]National Creative Research Initiatives Center for Adipose Tissue Remodeling, Institute of Molecular Biology and Genetics, Department of Biological Sciences, Seoul National University, Seoul, 08826, South Korea
[2]Department of Computer Science and Engineering, Seoul National University, Seoul, 08826, South Korea
[3]Department of Biophysics and Chemical Biology, Seoul National University, Seoul, 08826, South Korea
[4]Division of Endocrinology, Metabolism and Diabetes, Department of Medicine, University of Massachusetts Medical School, Worcester, MA, USA
[5]Obesity Research Center, College of Medicine, King Saud University, Riyadh 11461, Saudi Arabia

Correspondence to Jae Bum Kim
Email: jaebkim@snu.ac.kr

This PDF file includes:

MATERIALS AND METHODS

Animals

Six-week-old C57BL6/J male- and female- mice, and C57BLKS/J-Lepr^{db}/Lepr^{db} (*db/db*) male mice were purchased from Central Lab Animal Inc. (Seoul, Korea). Ds-Red^{+} transgenic mice were generously provided by Gou Young Koh (KAIST, Daejeon, South Korea). The mice were housed in colony cages under 12 h light/12 h dark cycles with free access to food and water. At eight weeks of age, male mice were fed HFD containing 60% kcals of fat (Research Diets Inc., New Brunswick, NJ, USA) with free access to drinking water. All experiments were approved by the Seoul National University Institutional Animal Care and Use Committees.

Human samples

Human adipose tissue samples were obtained from the Obesity Research Center at the College of Medicine, King Saud University, Riyadh, Saudi Arabia. The protocol was approved by the College of Medicine Ethics Committee, King Saud University (approval code 07-602), in accordance with the Declaration of Helsinki. Written informed consent was obtained from all participants prior to enrollment in the study.

Chemicals treatments

For animal experiments, 50 mg/kg of GABA (A2129; Sigma-Aldrich, St. Louis, MO, USA) and 1.5 mg/kg of Sac (0246; Tocris, Bristol, UK), a selective $GABA_B$ antagonist, were intraperitoneally injected into mice. For *ex-vivo* condition, GABA (100 nM) and Bac (10 μM), a $GABA_B$ receptor agonist, were used. Sac (20 μM) and another $GABA_B$ receptor antagonist CGP (50 μM) (1245; Tocris) were used in the *ex-vivo* monocyte migration assay. Bicuculline methiodide (Bicu; 50 μM) (2503; Tocris) was utilized to inhibit $GABA_A$ receptor-mediated signaling.

RNA-sequencing analyses

mRNAs from adipocytes and SVCs from obese EAT or obese IAT were prepared for the RNA-sequencing libraries. Then, all the libraries were sequenced with 101-bp paired-ends on an Illumina HiSeq instrument (Macrogen^{TM}, Seoul, South Korea). Read pairs were aligned using RSEM v.1.2.25 (1) and Bowtie 2.2.6 (2) to the *Mus musculus* genome (GRCm38/mm10) (3). We estimated the expected number of fragments from each transcript and gene with RSEM. Limma (Voom) (4) was used to perform statistical tests for pairwise differential expression between samples (EAT and IAT; NCD and HFD), calculate $\log_2$ fold change ($\log_2$FC) values and select DEGs with adjusted *p*-value cutoff <0.05.

Pathway analysis

Signaling pathway impact analysis (SPIA) (5) was used for pathway analysis. Three-hundred fourteen pathways annotated in the Kyoto Encyclopedia of Genes and Genomes (KEGG) database (6) were analyzed. Among the three statistics (pNDE: *p*-value from the number of DEGs, pPERT: *p*-value from perturbation factor, pINT: integrated *p*-value of pNDE and pPERT) generated by SPIA, the significance of pathways was determined based on pINT. The average absolute log fold change of pathway genes and pINT were used to generate half-volcano plots of pathways. Among the pathways in a half-volcano plot, pathways on the upper-right frontline (with more significant *p*-values and higher fold changes) were selected by Pareto optimization (7). Comparing the IAT-SVC with the EAT-SVC group, six pathways were included in the Pareto optimal set, excluding pathways below 1.0 and $-\log_{10}(0.05)$ for the x and y-axis, respectively. Selected pathways and their differentially expressed genes were visualized as a bipartite graph using Cytoscape software (8).

Body composition and hyperinsulinemic-euglycemic clamp

Male C57BL/6J mice fed a HFD for 9 weeks (15 weeks of age) were purchased from JAX (Bar Harbor, ME, USA), and after 1 week of acclimation, whole-body fat and lean mass were measured using proton magnetic resonance spectroscopy (^{1}H-MRS; Echo Medical Systems, Houston, TX, USA) at the

National Mouse Metabolic Phenotyping Center (MMPC) at the University of Massachusetts Medical School (Worcester, MA, USA). All mice received a daily intraperitoneal injection of GABA (50 mg/kg body weight) or vehicle (phosphate buffered saline [PBS] as a controls) for 2 weeks with continuous feeding of HFD. A 2 h hyperinsulinemic-euglycemic clamp was performed to measure insulin sensitivity and glucose metabolism in awake mice as previously described (9). Briefly, a survival surgery was performed at 5~6 days before clamp experiments to establish an indwelling catheter in the jugular vein. On the day of clamp experiments, mice were fasted overnight (~15 h), and the clamp experiment began with a primed and continuous infusion of human insulin (150 mU/kg body weight priming followed by 2.5 mU/kg/min; Novolin®, Novo Nordisk, NJ, USA). To maintain euglycemia, 20% glucose was infused at a variable flow rate during the clamp. Insulin-stimulated whole-body glucose metabolism was assessed using a continuous infusion of [3-^{3}H] glucose (PerkinElmer, Waltham, MA, USA), and 2-[^{14}C] deoxyglucose was injected at 75 min of clamp to assess glucose uptake in individual organs.

Adipose tissue fractionation and flow cytometry

Adipose tissue was fractionated as previously described (10). Briefly, EAT and IAT were chopped and incubated in collagenase buffer at 37℃ with shaking for 30 min. After centrifugation, adipocytes in the supernatant were collected. Simultaneously, the pelleted SVCs were incubated with red blood cell lysis buffer (a 1:9 mixture of 0.17 M Tris (pH 7.65) and 0.16 M NH_4Cl), centrifuged at 1,300 rpm for 5 min, and resuspended in PBS to remove red blood cell-derived components. In turn, the SVCs were stained with monoclonal antibodies against CD11b (BD Biosciences, San Jose, CA, USA), F4/80 (eBioscience, San Diego, CA, USA), and CD11c (eBioscience) at 4℃ for 30 min. After staining of the ATM surface markers, Ki67 (eBioscience) or Annexin V (BD Biosciences) antibody staining was performed, following the manufacturer's protocols. For the analysis of ADSCs, SVCs were incubated with antibodies against CD31 (eBioscience), CD34 (eBioscience), and Sca-1 (eBioscience). After incubation, the cells were gently washed and resuspended in PBS. The stained cells were analyzed or sorted for ADSCs using the FACS Canto II™ or FACS Aria II™ instrument (BD Biosciences). Primary adipocyte

size was measured using a BioSorter™ (Union Biometrica, Holliston, MA, USA)

Measurement of *in vivo* ATM infiltration

To isolate leukocyte pools from Ds-Red$^+$ transgenic mice, blood was collected by heart puncture in 1.5 mL tube and was mixed with 20 μL of 0.5 M EDTA to prevent blood clotting. Blood samples were pooled to 3 mL in a Greiner Leucosep tube (GN163290; Sigma Aldrich) pre-equilibrated with 3 mL of NycoPrep 1.077 (1114550; Axis-Shield PoC AS, Oslo, Norway). After centrifugation at 2,500 rpm and at room temperature for 10 min, the middle layer was carefully isolated and washed with RoboSep buffer (20104; STEMCELL Technologies, Vancouver, Canada). MNCs (1×10^6) in RoboSep buffer were intravenously injected into mice. After a resting period, each fat tissue was extracted from the recipient mice to examine exogenous MNC infiltration into adipose tissues.

Adipose tissue and ADSC transplantation

Littermates fed NCD or HFD for 10 weeks were used as recipients, and age-matched HFD-fed mice were used as donors. Fat transplantation was performed using fat pads from EAT and IAT. Isolated adipose tissues were fragmented into approximately 0.6 g for transplantation into visceral loci or 0.3 g for transplantation into subcutaneous loci. Each adipose fragment was kept in an incubator 37℃ in 3 mL of PBS until transplantation. Recipient mice were anesthetized by injection of 0.2 mL/kg Rompun and 0.4 mL/kg Zoletil in PBS (200 μL). For adipose tissue transplantation, one fat slice was transplanted into EAT and IAT of recipient mice. In the sham group, fat tissue was not transplanted. For ADSC transplantation, CD31$^-$, CD34$^+$, and Sca-1$^+$ ADSCs were collected from either IAT or EAT and resuspended in RoboSep™ buffer (STEMCELL Technologies). IAT-ADSCs (3×10^5) or the same number of EAT-ADSCs were injected into the EAT in the right flanks of individual HFD-fed mice of each group. In EAT in the left flank, RoboSep™ buffer was injected as a vehicle.

Whole mount immunohistochemistry

Adipose tissues were mounted after fixation by vascular perfusion of 1% paraformaldehyde in PBS. The whole-mounted tissues were incubated with a blocking solution containing 5% goat serum (005-000-121; Jackson ImmunoResearch, West Grove, PA, USA) in 0.3% PBS-T at room temperature for 1 h. After blocking, the whole-mounted adipose tissues were incubated with antibodies against CD31 (MAB1398Z; Merck, Billerica, MA, USA), CD11b (14-0112-81; eBioscience), and CD11c (14-0114-81; eBioscience) at 4°C overnight. After several washes with PBS-T, the whole-mounted tissues were incubated with secondary antibodies, namely FITC, Cy3- or Cy5-conjugated anti-Armenian hamster antibody, anti-rat antibody or anti-rabbit antibody (diluted 1:500; Jackson ImmunoResearch) at room temperature for 1 h. Lipid droplets in adipocytes were visualized by coherent anti-strokes Raman scattering (CARS) microscopy (TCS SP8 CARS microscope, Leica Microsystems, Wetzlar, Germany). Pump and Strokes lasers were tuned to 14,140 cm^{-1} (or 707 nm) and 11,300 cm^{-1} (or 885 nm), respectively, to be in resonance with the CH_2 symmetric stretch vibration at 2,840 cm^{-1}. Glucose bioprobe (GB-Cy3) was stained as previously studied (11). The signals were visualized and digital images were obtained using a Zeiss LSM700 (Carl Zeiss, Oberkochen, Germany) or a Leica TCS SP8 CARS microscope (Leica Microsystems).

Monocyte migration assay

Monocyte migration was assayed as previously described (12). Briefly, THP-1 monocytes or mouse monocyte from blood was pre-stained with 2 μM of Cell Tracker™-CMPTX (C34552; Thermo Fisher Scientific, Waltham, MA, USA) at 37℃ for 1 h and then washed with PBS. CM from each sample were loaded to the lower layer of 8-μm pore-size Trans-well insert (CLS3428; Sigma-Aldrich). In each sample group, 3×10^5 THP-1 cells were loaded on the upper surface of upper layer of Trans-well insert. After 12 h or 48 h of incubation, upper layer was removed. Then the chemotactic cells were stained with Hoechst dye (H3570; Thermo Fisher Scientific) for 30 min. After removal of the dye by washing, 10% FBS high-glucose DMEM was added, and the plates were observed under the LSM700 confocal microscope. In randomized microscope images, cells positive for Cell-Tracker™ (red) and Hoechst (blue) were counted and quantified.

GABA measurement

EAT and IAT samples were homogenized in 2 mL of PBS. After centrifugation at 12,000 rpm and at 4℃ for 10 min, the middle layer was carefully isolated. Tissue extracts in PBS were mixed with 10% trichloroacetic acid in cold acetone (1:4 ratio v/v) and incubated overnight at –20℃ freezer. To remove proteins, the samples were centrifuged at 14,000 rpm and at 4℃ for 30 min. The supernatants were carefully taken and dried in a SpeedVac^{TM} (Thermo Fisher Scientific). Dried samples were reconstituted with 0.1% formic acid in distilled water and analyzed by liquid chromatography-mass spectrometry at the National Instrumentation Center for Environmental Management (Seoul, South Korea).

Western blot analyses

Isolated EAT and IAT samples were homogenized in modified immunoprecipitation assay (RIPA) buffer (50 mM Tris-HCl [pH 7.4], 150 mM NaCl, 1 mM EDTA, 1 mM PMSF, 1% (v/v) NP-40, 0.25% (w/v) Na-deoxycholate, protease inhibitor cocktail with 1 mM NaF, and 10 mM Na_3VO_4 as phosphatase inhibitor) and subjected to 8% SDS-PAGE. The following antibodies were used: phosphorylated Akt (pAkt^{S473}) (9271; Cell Signaling Technology, Danvers, MA, USA), Akt (9272; Cell Signaling Technology), phosphorylated GSK3β (pGSK3β^{S9}) (9336; Cell Signaling Technology), GSK3β (610201; BD bioscience), and β-actin (A5411; Sigma-Aldrich). For assessment of inflammatory signaling, phosphorylated c-Jun N-terminal kinase (pJNK) (SC6254; Santa Cruz Biotechnology, Dallas, TX, USA), JNK (SC474; Santa Cruz Biotechnology), phosphorylation of p38 mitogen-activated protein kinase (pp38) (9211; Cell Signaling Technology), p38 (9212; Cell Signaling Technology), and β-actin (A5316; Sigma-Aldrich) antibodies were used.

***in vivo* GSIS**

24 h fasted mice were injected with glucose (2 g/kg), and tail blood was collected before, and at 10 and 20 min after injection. Blood was centrifuged for 10 min at 6,000 rpm (4℃) to collect plasma. Blood

insulin concentration was determined using mouse insulin ELISA kit (Morinaga Institute of Biological Science, Yokohana, Japan).

Glucose and insulin tolerance test

For glucose tolerance testing, 6 h or 24 h fasted mice were intraperitoneally injected with glucose (2 g/kg glucose, 20% glucose solution) as previously reported (13). For insulin tolerance test, mice were intraperitoneally injected with insulin (0.5 U/kg). Blood samples were drawn at 15, 30, 60, 90, and 120 min after glucose or insulin injection by taking 3 μL of blood collected from the tip of the tail vein. To determine HOMA-IR, mice were fasted for 6 h and blood was taken from each experimental group. Insulin levels were measured using a mouse insulin ELISA kit (AKRIN-011T; Shibayagi, Gunma, Japan).

RNA isolation and qRT-PCR

Tissues were homogenized in TRIzol reagent (Molecular Research Center, OH, USA) as described previously (14). cDNA was synthesized with M-MuLV reverse transcriptase (Fermentas, MD, USA). The cDNA was mixed with TOPreal^{TM} qPCR 2X PreMIX (RT500M; Enzynomics, Daejeon, South Korea). qRT-PCR was performed using the CFX96^{TM} real-time system (Bio-Rad Laboratories, CA, USA). The threshold cycle (Ct) values of each mRNA were normalized to average Ct value of cyclophilin mRNA. The primers used for qRT-PCR in this study were synthesized by Bioneer (Daejeon, South Korea).

Statistical analysis

Data are presented as the mean ± SEM. Differences between two groups were assessed using Student's *t*-test. Means of more than two groups were compared by ANOVA (GraphPad Prism; GraphPad, San

Diego, CA, USA) followed by *post-hoc* tests (one-way; Tukey, two-way; Bonferroni). Pearson's test was used to calculate correlation coefficients between BMI and mRNA levels.

REFERENCE

1. Li B & Dewey CN (2011) RSEM: accurate transcript quantification from RNA-Seq data with or without a reference genome. *Bmc Bioinformatics* 12.
2. Langmead B & Salzberg SL (2012) Fast gapped-read alignment with Bowtie 2. *Nat Methods* 9(4):357-359.
3. Waterston RH, *et al.* (2002) Initial sequencing and comparative analysis of the mouse genome. *Nature* 420(6915):520-562.
4. Law CW, Chen YS, Shi W, & Smyth GK (2014) voom: precision weights unlock linear model analysis tools for RNA-seq read counts. *Genome Biol* 15(2).
5. Tarca AL, *et al.* (2009) A novel signaling pathway impact analysis. *Bioinformatics* 25(1):75-82.
6. Kanehisa M & Goto S (2000) KEGG: Kyoto Encyclopedia of Genes and Genomes. *Nucleic Acids Res* 28(1):27-30.
7. Fleming CMFaPJ (1993) Genetic Algorithms for Multiobjective Optimization: Formulation, Discussion and Generalization. *Proceedings of the 5th International Conference on Genetic Algorithms*:416-423.
8. Shannon P, *et al.* (2003) Cytoscape: A software environment for integrated models of biomolecular interaction networks. *Genome Res* 13(11):2498-2504.
9. Kim JK (2009) Hyperinsulinemic-euglycemic clamp to assess insulin sensitivity in vivo. *Methods Mol Biol* 560:221-238.
10. Huh JY, *et al.* (2013) A Novel Function of Adipocytes in Lipid Antigen Presentation to iNKT Cells. *Mol Cell Biol* 33(2):328-339.
11. Kim JI, *et al.* (2015) Lipid-Overloaded Enlarged Adipocytes Provoke Insulin Resistance Independent of Inflammation. *Mol Cell Biol* 35(10):1686-1699.
12. Lee YS, *et al.* (2010) Adipocytokine Orosomucoid Integrates Inflammatory and Metabolic Signals to Preserve Energy Homeostasis by Resolving Immoderate Inflammation. *J Biol Chem* 285(29):22174-22185.
13. Choe SS, Shin KC, Ka S, Lee YK, & Kim JB (2014) Macrophage HIF-2 Alpha Ameliorates Adipose Tissue Inflammation and Insulin Resistance in Obesity. *Diabetes* 63:A50-A50.
14. Jeong HW, *et al.* (2010) A nonthiazolidinedione peroxisome proliferator-activated receptor alpha/gamma dual agonist CG301360 alleviates insulin resistance and lipid dysregulation in db/db mice. *Molecular pharmacology* 78(5):877-885.

Fig. S1.

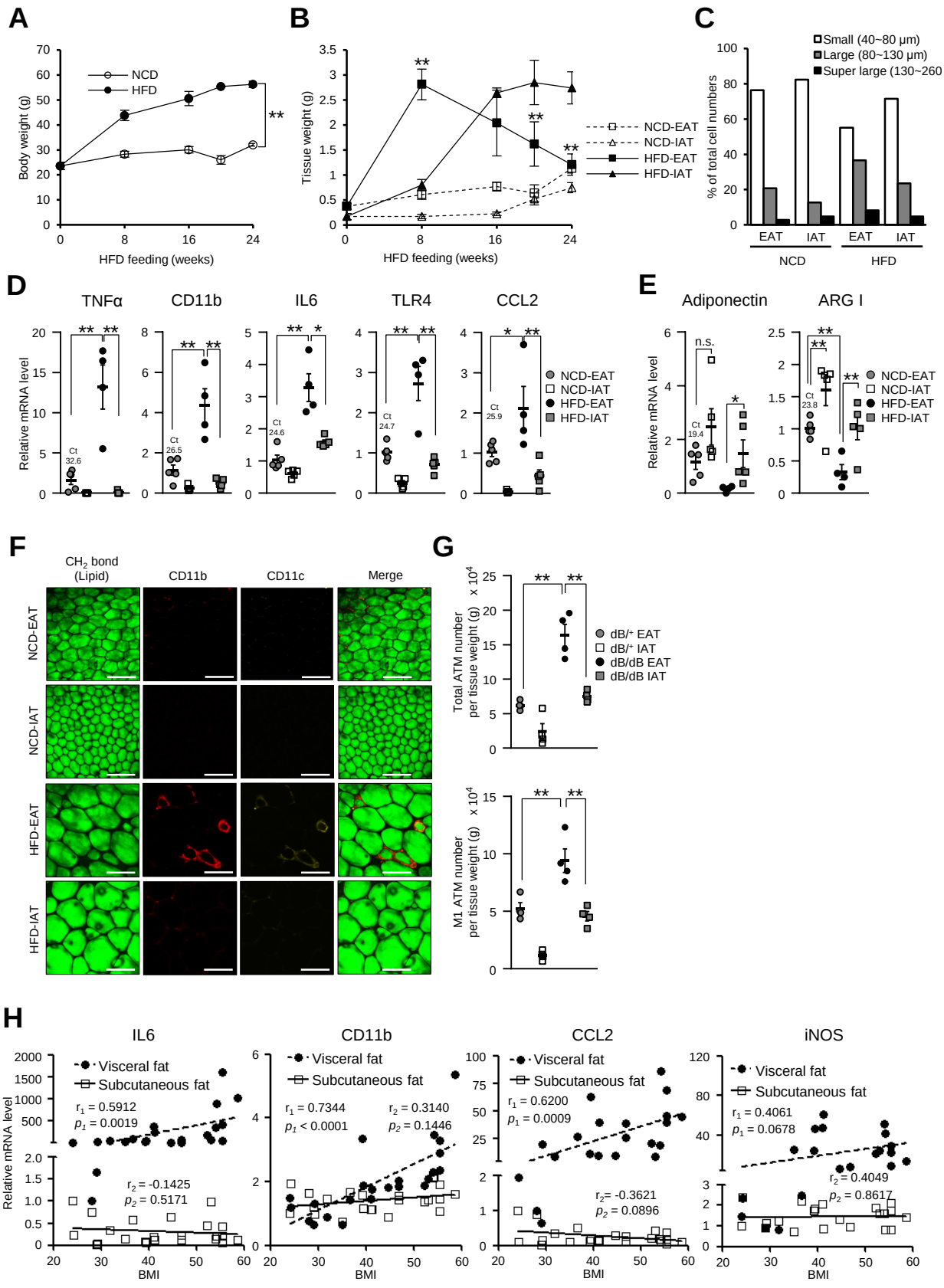
A
Body weight (g)
HFD feeding (weeks)
NCD
HFD
B
Tissue weight (g)
HFD feeding (weeks)
NCD-EAT
NCD-IAT
HFD-EAT
HFD-IAT
C
% of total cell numbers
Small (40~80 μm)
Large (80~130 μm)
Super large (130~260 μm)
EAT
IAT
NCD
HFD
D
TNFα
CD11b
IL6
TLR4
CCL2
Relative mRNA level
E
Adiponectin
ARG I
n.s.
F
CH2 bond (Lipid)
CD11b
CD11c
Merge
NCD-EAT
NCD-IAT
HFD-EAT
HFD-IAT
G
Total ATM number per tissue weight (g) x 10^4
M1 ATM number per tissue weight (g) x 10^4
dB/+ EAT
dB/+ IAT
dB/dB EAT
dB/dB IAT
H
IL6
CD11b
CCL2
iNOS
Visceral fat
Subcutaneous fat
Relative mRNA level
BMI

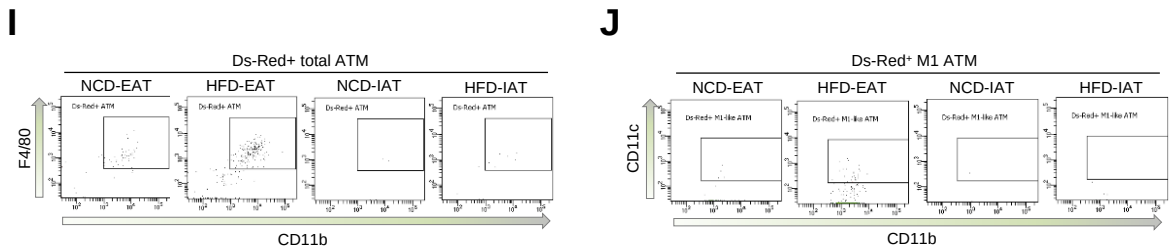

Fig. S1. Differential aspects of body weights, adiposity, and inflammatory responses in mice and in human fat-depots
(A) Body-weight changes in NCD and HFD-fed mice. At 0, 8, 16, 20, and 24 weeks after NCD or HFD feeding, body weight was measured. n = 4 for each group. **(B)** IAT and EAT weights were measured for 24 weeks. n = 4 for each group. **(C)** Distribution of adipocyte sizes. The sizes of isolated adipocytes were measured, and cells were counted using BioSorter^{TM}. **(D)** Relative mRNA levels of inflammatory proteins, including TNFα, CD11b, IL6, TLR4, and CCL2. Average Ct values for NCD-EAT are denoted. **(E)** Relative mRNA levels of anti-inflammatory proteins, including adiponectin and arginase (ARG) I. Average Ct values of NCD-EAT are denoted. (**F)** Representative whole-mount images of CD11b^{+} (Red) and CD11c^{+} (Yellow) in IAT and EAT from NCD- and HFD-fed mice. Adipose tissue lipid droplets (green) were visualized by TCS SP8 CARS microscopy. Scale bar indicates 100 μm. **(G)** Flow-cytometric analysis of fat depot-selective accumulation of ATMs (upper panel) and M1-like ATMs (lower panel) in *db/db* mice. **(H)** Correlation of mRNA levels of IL6, CD11b, CCL2 and inducible nitric oxide synthase (iNOS) in human subcutaneous and visceral adipose tissues correlated with body mass index (BMI). **(I and J)** Representative flow cytometric images of **(I)** Ds-Red^{+}, CD11b^{+} and F4/80^{+} exogenous ATM and **(J)** Ds-Red^{+}, CD11b$^{+,}$ F4/80^{+}, and CD11c^{+} exogenous M1-like ATM. Error bars represent means ± SEs of treatment groups. **p* < 0.05, ***p* < 0.01, n.s., not significant. Pearson's correlation coefficient (r_1 and r_2), and *p*-values (p_1 *and* p_2) are indicated. r_1 and p_1 indicate the values of visceral adipose tissue, and r_2 and p_2 denote the values of subcutaneous adipose tissue. BMI ranged from 24.11 to 58.80 kg/m^2 (n = 23, or n = 21 for iNOS measurement). For panel **(D and E)**, eight-week old mice were fed HFD for ten weeks before sacrifice.

Fig. S2.

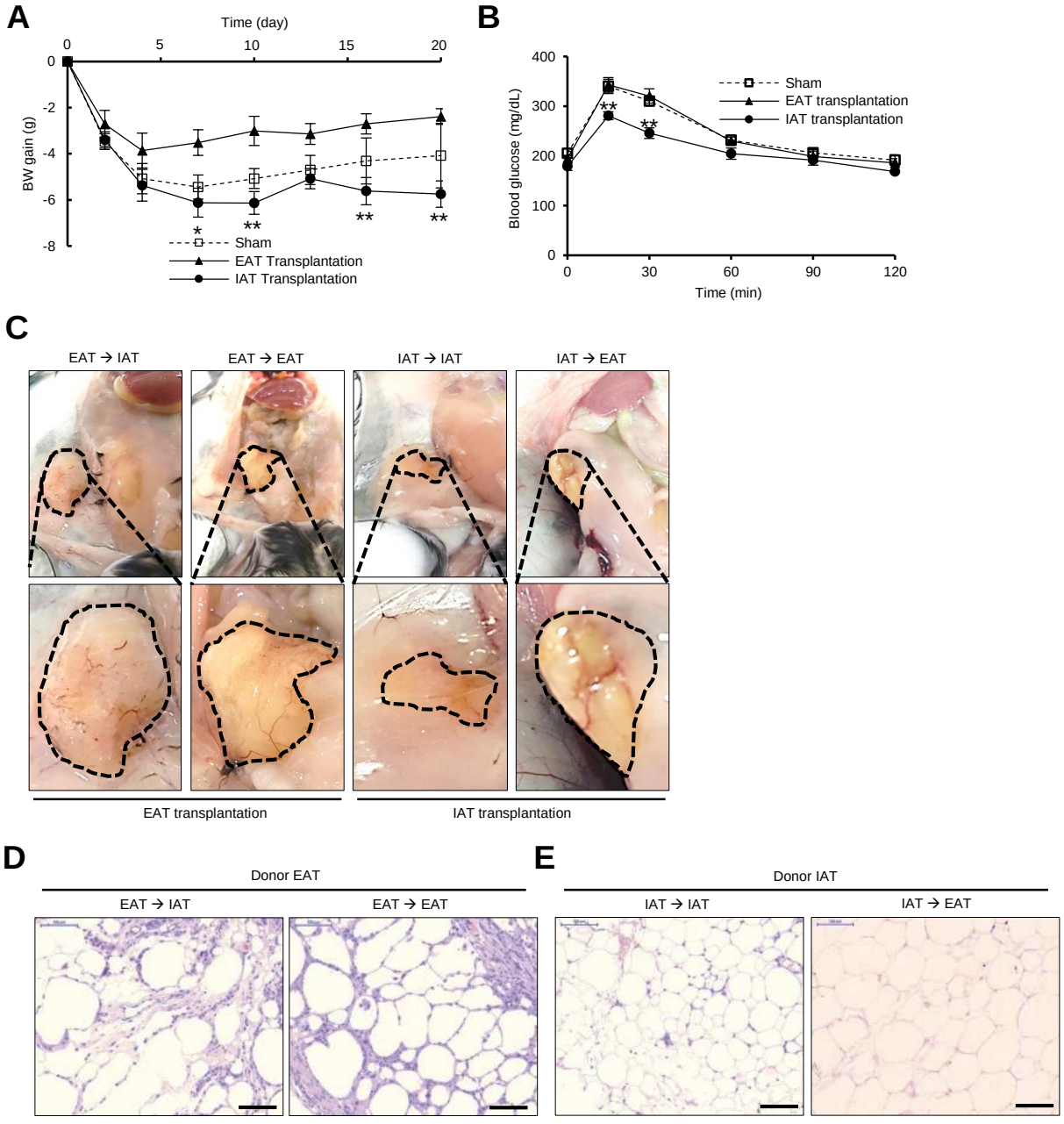

Fig. S2. The effects of EAT and IAT transplantation
After adipose tissue transplantation, body-weight changes and glucose tolerance were measured in each recipient mouse group. **(A)** Body weight changes were measured until 20 days after adipose tissue transplantation. **(B)** At two weeks after adipose tissue transplantation, 6 h fasted mice were tested for glucose tolerance. **(C)** Representative images of transplanted donor adipose tissues in recipient mice at three weeks after surgery. Black dotted lines indicate donor adipose tissues. **(D and E)** Representative images of hematoxylin and eosin-stained **(D)** donor EAT and **(E)** donor IAT. Scale bars indicate 100 μm. *$p < 0.05$, **$p < 0.01$ vs. sham.

Fig. S3.

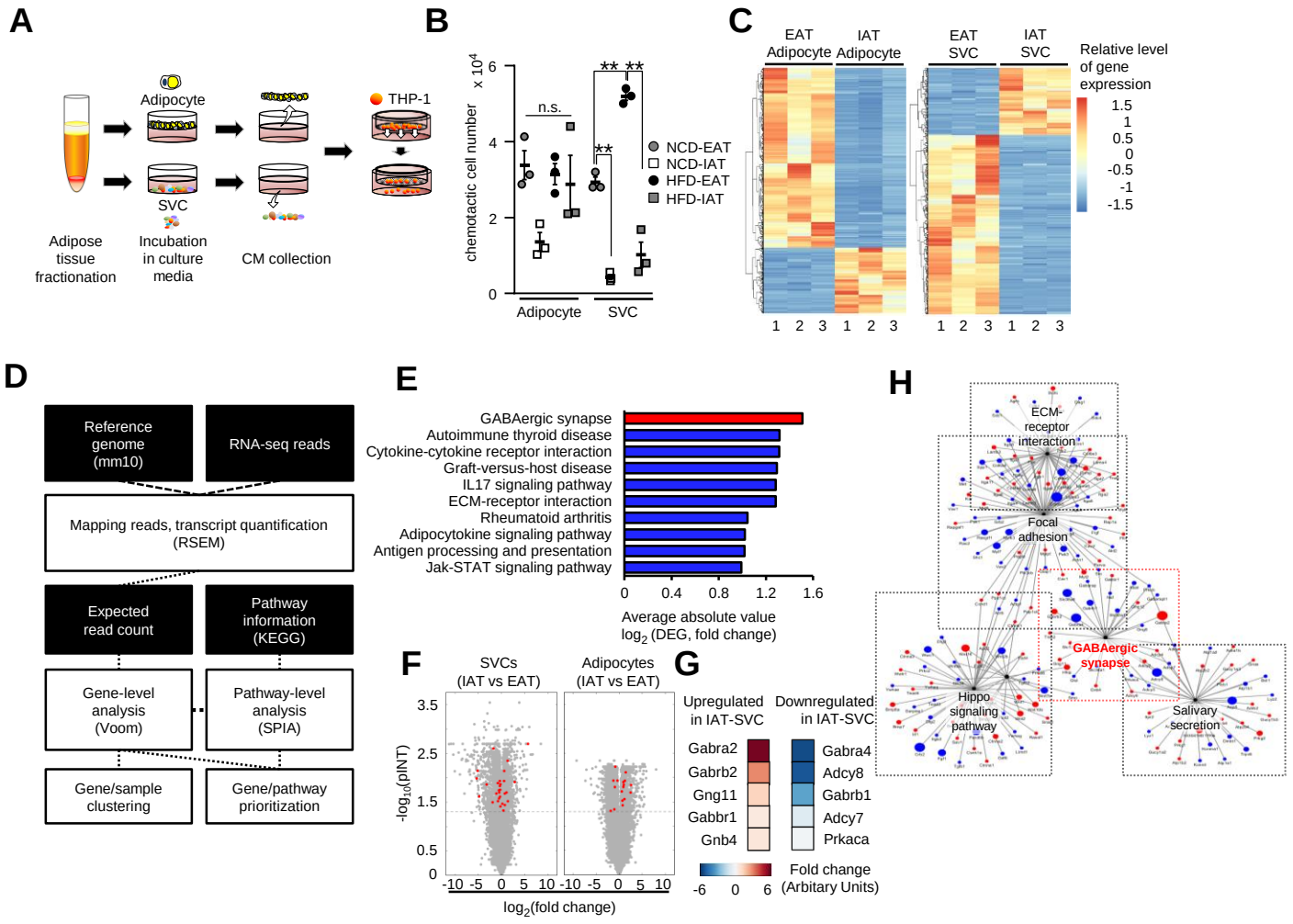

Fig. S3. Distinct patterns of monocyte migration and transcriptome between adipocytes and SVCs from IAT and EAT
(A) An experimental strategy used to test monocyte migration by using CM from adipocytes and SVCs. **(B)** Migrated monocytes were counted in adipocytes or SVCs from NCD-EAT, NCD-IAT, HFD-EAT, and HFD-IAT. **(C)** Heat-maps displaying expression patterns of DEGs between EAT and IAT in adipocytes and SVCs. Genes are represented by horizontal lines and were hierarchically clustered on the basis of z-transformed expression patterns. **(D)** Algorithms of RNA-sequencing data analyses. RNA-sequencing reads were aligned to the *Mus musculus* genome (GRCm38/mm10) and expected read counts for genes and transcripts were estimated by RSEM. Expected read counts were used for gene-level analysis in Limma (Voom), which performs statistical tests of differential expression and estimates the fold change and significance (*p*-value) of genes. Pathway information from the KEGG database was integrated with gene-level statistics from Limma (Voom) to rank and prioritize significant biological pathways that showed signaling propagation. **(E)** Comparisons of fold changes in gene expression in KEGG pathways related to immunity, inflammation, and GABAergic synapse between IAT-SVCs and EAT-SVCs of DIO. **(F)** Volcano plots of individual genes in SVCs (left) and adipocytes (right) from IAT and EAT. DEGs involved in GABAergic synapse are depicted as red dots. **(G)** Presentation of color-coded top DEGs among GABAergic synapse genes. **(H)** A bipartite graph of functional enrichment analyses using data sets comparing obese IAT-SVC and obese EAT-SVC groups. Black nodes represent individual enriched pathways with high average fold changes and significant *p*-values selected as the Pareto-optimal set of pathways. Genes upregulated and downregulated in IAT-SVCs are indicated as red and blue spots, respectively, the size of which corresponds to relative fold change. n = 3 for each experimental group for analysis of RNA-sequencing. The *x*-axis of the bar plot denotes the score ($\log_2$) of average fold changes of DEGs in a single pathway. Error bars represent means ± SEs of treatment groups. $^{**}p < 0.01$, n.s., not significant.

Fig. S4.

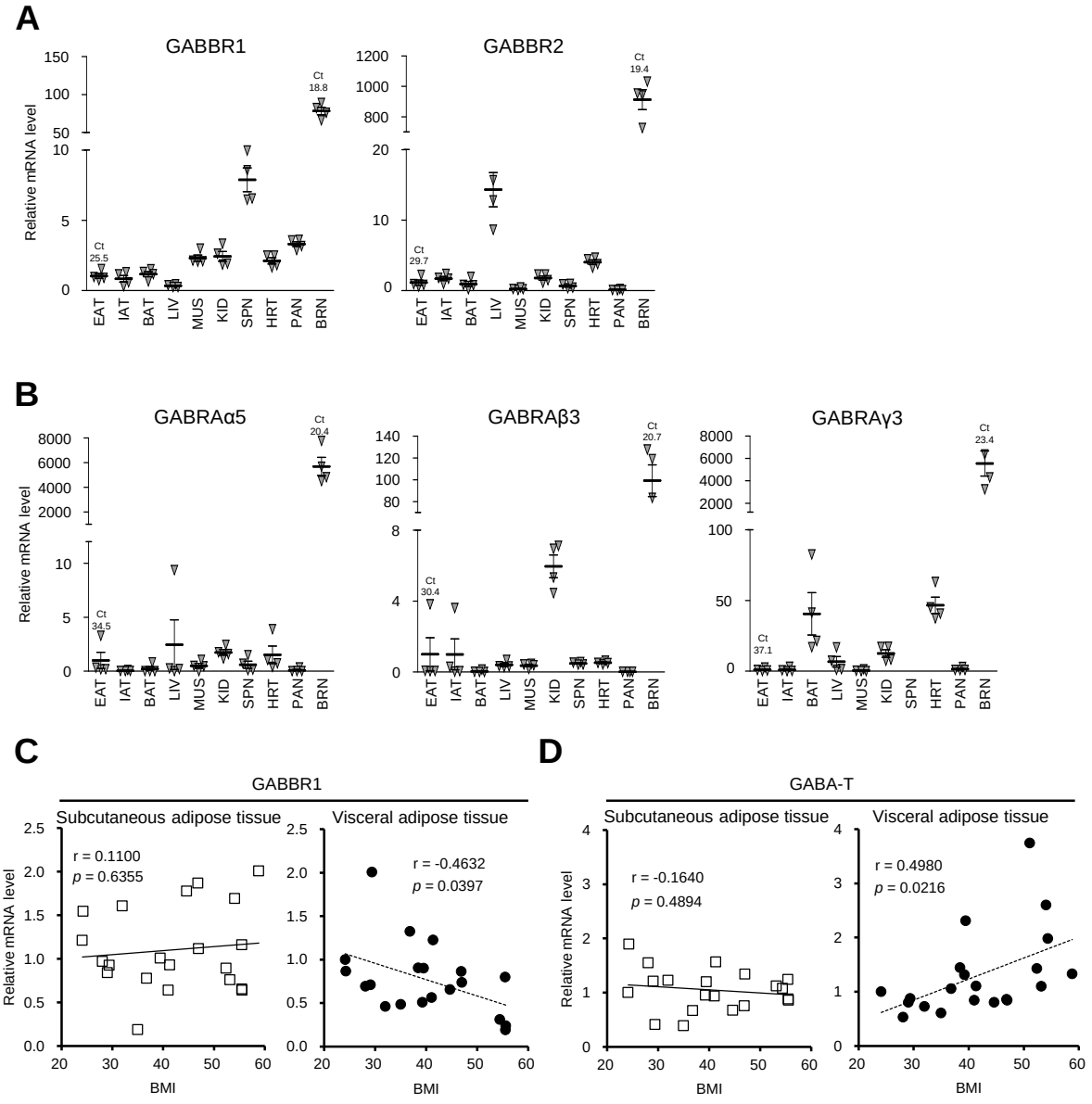

Fig. S4. The mRNA expression of GABA related genes in various mouse tissues and humans
(A and B) Measurement of GABA receptor gene expression in various mouse tissues. **(A)** $GABA_B$ receptor genes, and **(B)** $GABA_A$ receptor subunits in various tissues: "BAT," brown adipose tissue; "LIV," liver; "MUS," muscle; "KID," kidney; "SPN," spleen; "HRT," heart; "PAN," pancreas; and "BRN," brain. **(C and D)** mRNA level correlation of **(C)** GABBR1 and **(D)** GABA-T in human subcutaneous (left) and visceral adipose tissues (right) with BMI. BMI ranged from 24.11 to 55.55 kg/m^2, n = 21. Pearson's correlation coefficient (r) and *p*-values (*p*) are indicated. For panel **(A and B)**, average Ct values of EAT and brain are denoted. Error bars represent means ± SEs of treatment groups

Fig. S5.

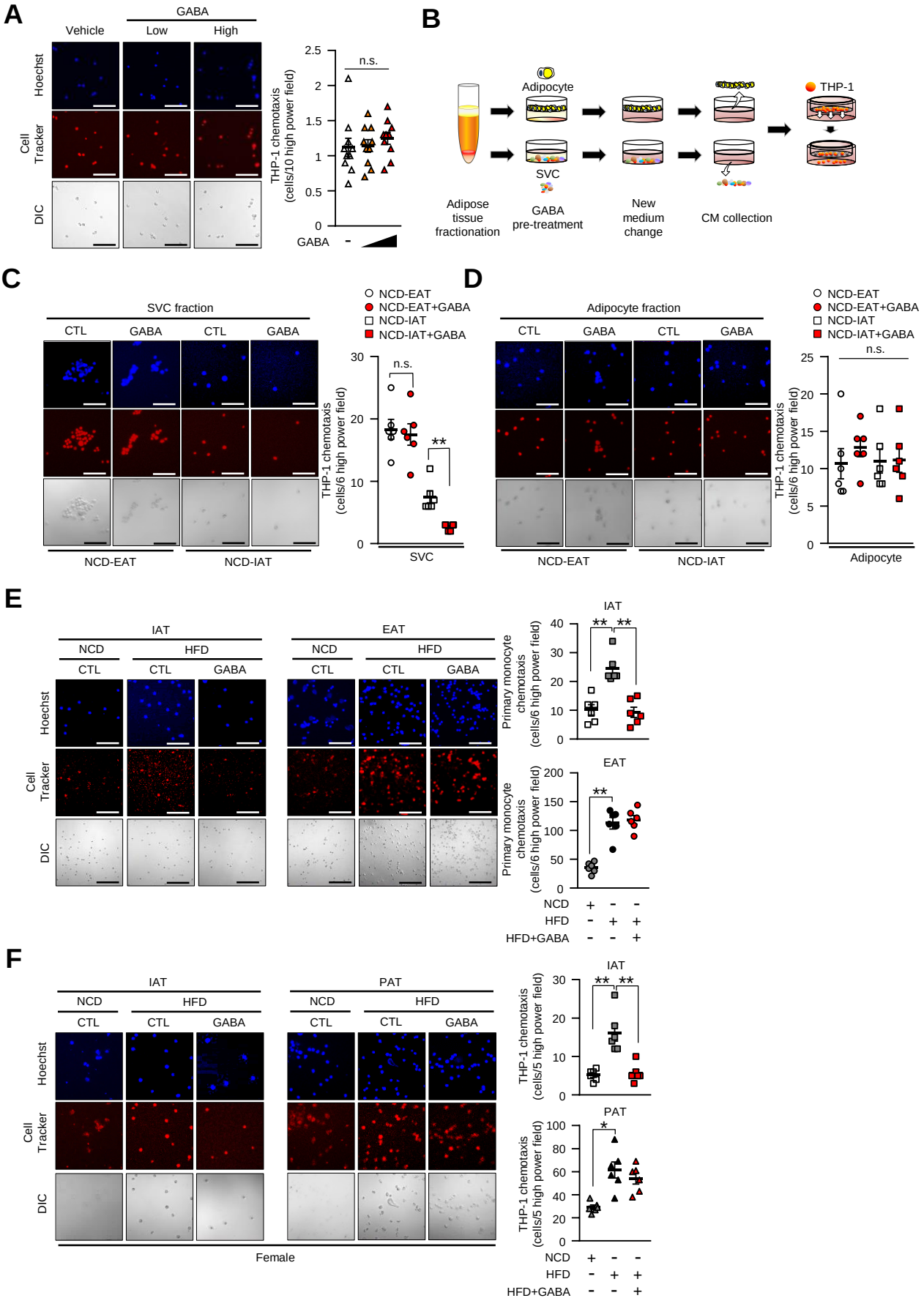
A
GABA
Vehicle
Low
High
Hoechst
Cell Tracker
DIC
THP-1 chemotaxis (cells/10 high power field)
n.s.
GABA
B
Adipocyte
SVC
THP-1
Adipose tissue fractionation
GABA pre-treatment
New medium change
CM collection
C
SVC fraction
CTL
GABA
NCD-EAT
NCD-EAT+GABA
NCD-IAT
NCD-IAT+GABA
THP-1 chemotaxis (cells/6 high power field)
n.s.
**
SVC
D
Adipocyte fraction
Adipocyte
E
IAT
EAT
NCD
HFD
Primary monocyte chemotaxis (cells/6 high power field)
F
PAT
THP-1 chemotaxis (cells/5 high power field)
*
Female
HFD+GABA

Fig. S5. Effects of GABA on monocyte migration and experimental strategy to study the effects of GABA-stimulated adipocytes and SVCs on monocyte migration

(A) Low (1 nM) and high (100 nM) dose of GABA in fresh media were used to measure THP-1 chemotaxis using an 8 μm-pore trans-well system. THP-1 monocytes were incubated in trans-well for 12 h. Representative images of migrated monocytes (left). n = 10 for each group were analyzed to calculate and average monocyte numbers (right). Scale bar indicates 100 μm. **(B)** Experimental strategy used to study monocyte chemotaxis in adipocytes and SVCs upon GABA treatment. **(C and D)** From the NCD-fed mice, IAT and EAT were fractionated into SVCs and adipocytes. To observe GABA effects on adipocytes and SVCs from NCD-fed mice, THP-1 was incubated in trans-well for longer period than the adipose samples from HFD-fed mice (48 h). Measurements of THP-1 monocyte migration in CM of GABA-treated **(C)** SVC fraction, and **(D)** adipocyte fraction. n = 6 for each experimental group. **(E)** Measurement of mouse primary monocyte migration in IAT (left) and EAT (middle). Quantification of monocyte migration from CM of GABA-stimulated IAT (upper right) and EAT (lower right). The mouse monocytes were incubated in trans-well for 12 h. n = 6 for each experimental group. Scale bar indicates 100 μm. **(F)** THP-1 chemotaxis in female IAT (left) and female PAT (middle). Quantification of monocyte migration from CM of GABA-stimulated IAT (upper right) and PAT (lower right). THP-1 was incubated in trans-well for 12 h. Scale bar indicates 100 μm. n = 6 for each experimental group. The number of migrated monocytes is indicated in the right panel of each figure. Scale bar indicates 100 μm. Error bars represent means ± SEs of treatment groups. *p<0.05 and **p < 0.01. n.s., not significant.

Fig. S6.

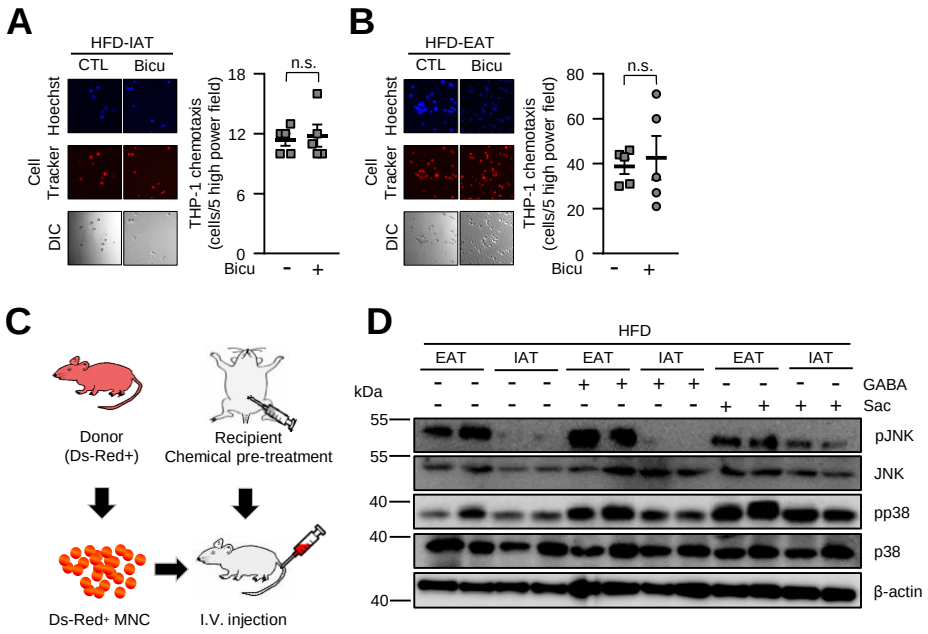

Fig. S6. The effect of $GABA_A$ and $GABA_B$ receptor modulations
(A and B) The inhibitory effect of $GABA_A$ receptor with Bicu in **(A)** IAT or **(B)** EAT on monocyte migration. THP-1 monocytes were incubated in trans-well for 12 h. The adipose-derived CM were collected from IAT or EAT. **(C)** A scheme of the *in vivo* ATM infiltration assay for $GABA_B$ receptor modulators in HFD-fed mice. Vehicle, GABA, or Sac was intraperitoneally injected twice prior to intravenous injection of Ds-Red^+ MNCs, and the mice were sacrificed at 12 h after chemical injection. **(D),** Western blot images of inflammatory signaling. Phosphorylated JNK (pJNK) and p38 (pp38) were measured in IAT and EAT upon GABA treatment. Total JNK, total p38, and β-actin were measured as controls. Error bars represent means ± SEs of treatment groups. n.s., not significant.

Fig. S7.

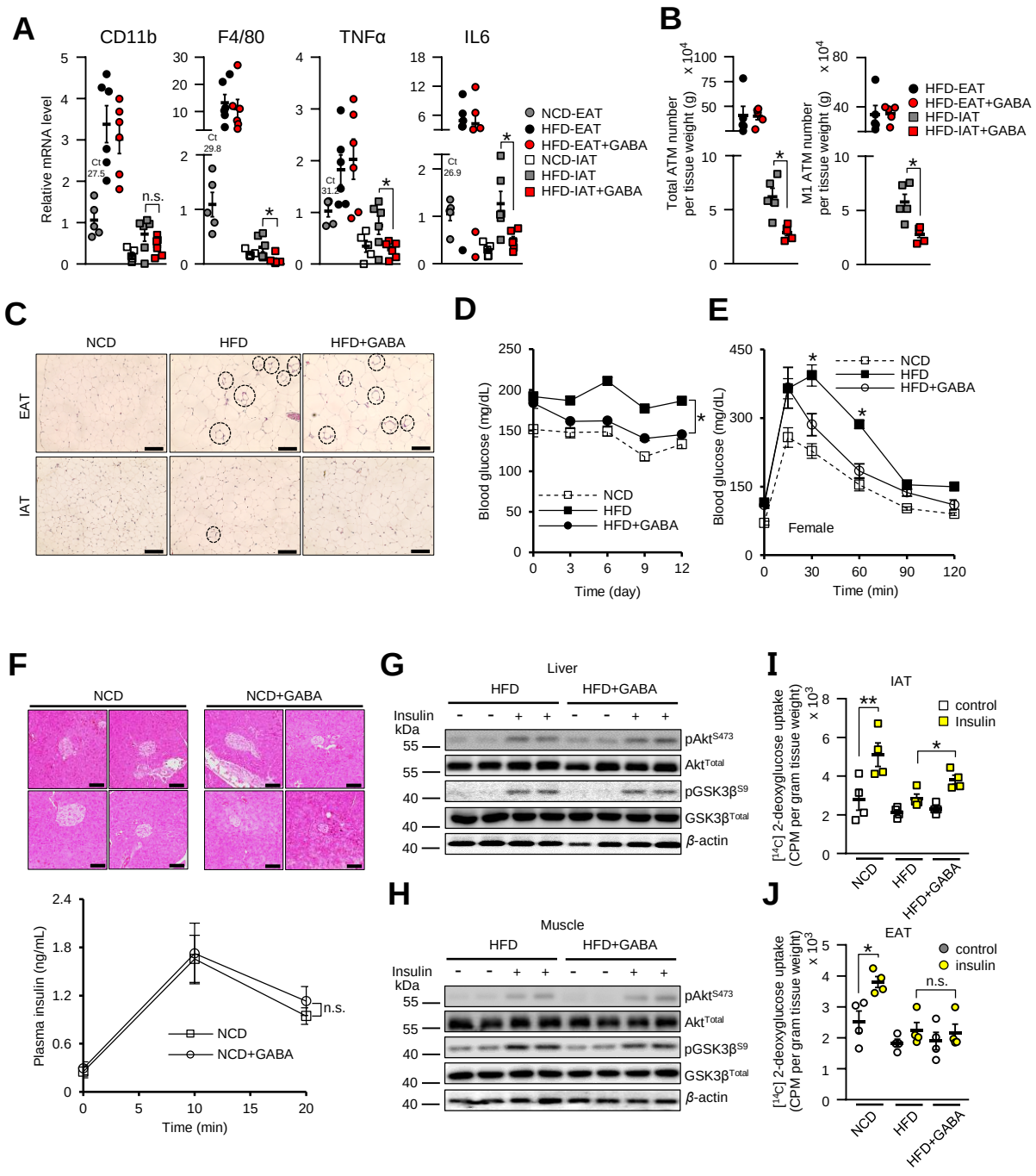

Fig. S7. GABA mediated inflammatory responses and metabolic changes in DIO mice

(A) Relative mRNA levels of ATM markers (CD11b and F4/80) and inflammatory cytokines (TNFα and IL6) in IAT and EAT of NCD, HFD, and HFD+GABA group. Average Ct values for NCD-EAT are denoted. **(B)** Flow-cytometric analysis of fat depot-selective accumulation of ATMs (left panel) and M1-like ATMs (right panel) in HFD-fed mice. **(C)** Representative images of hematoxylin and eosin-stained EAT and IAT. Each black circle indicates ATM (crown-like structures). Scale bars indicate 100 μm. **(D)** Blood glucose levels were measured every three days after GABA injection. **(E)** female mice with GABA treatment were intraperitoneally given glucose and measured the level of blood glucose in each time point. For panel n = 5 for each group. **(F)** Representative images of hematoxylin and eosin-stained pancreatic islet (upper panels) and *in vivo* GSIS (lower panels) from NCD-fed mice. For in vivo GSIS, n = 5 for each group. **(G and H)** Western blots for insulin signaling marker proteins in **(G)** liver and **(H)** muscle. Total Akt, total GSK3β, and β-actin were measured as controls. **(I and J)** Insulin-dependent [^{14}C] 2-deoxyglucose uptake was measured in **(I)** IAT and **(J)** EAT. n = 4 for each group. Error bars represent means ± SEs of treatment groups. *p < 0.05 (vs. HFD in panel B), n.s., not significant.

Fig. S8.

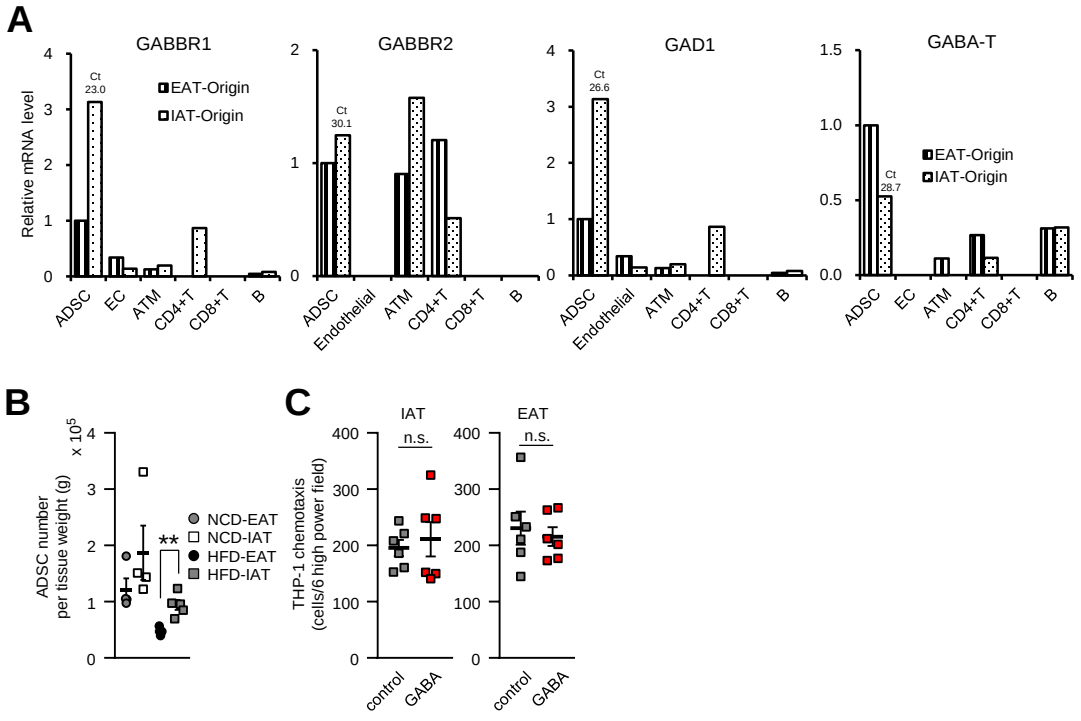

Fig. S8. The number of ADSCs and the effects of GABA stimulated CD4⁺ T_H cells on monocyte migration
(A) Relative mRNA levels of GABBR1, GABBR2, GAD1, and GABA-T in SVC-comprising cells of HFD-fed mice, including ADSCs ($CD31^-$, $CD34^+$, $Sca\text{-}1^+$), endothelial cells (ECs; $CD31^+$), ATM, $CD4^+$ T cells ($CD3^+$, $CD8^-$, and $CD4^+$), $CD8^+$ T cells ($CD3^+$, $CD4^+$, and $CD8^+$), and B cells ($CD3^-$ and $B220^+$). Average Ct values for each gene in IAT-ADSCs are denoted. **(B)** ADSCs were counted by flow cytometry. Total ADSC numbers were normalized by gram fat mass in each fat depot from NCD- and HFD-fed mice. **(C)** Measurement of migrated monocytes in response to CM of $CD4^+$ T cells from IAT (left) and EAT (right) upon GABA treatment. THP-1 monocytes were incubated in trans-well for 12 h. Error bars represent means ± SEs of treatment groups. $^{**}p < 0.01$, n.s., not significant.

Fig. S9.

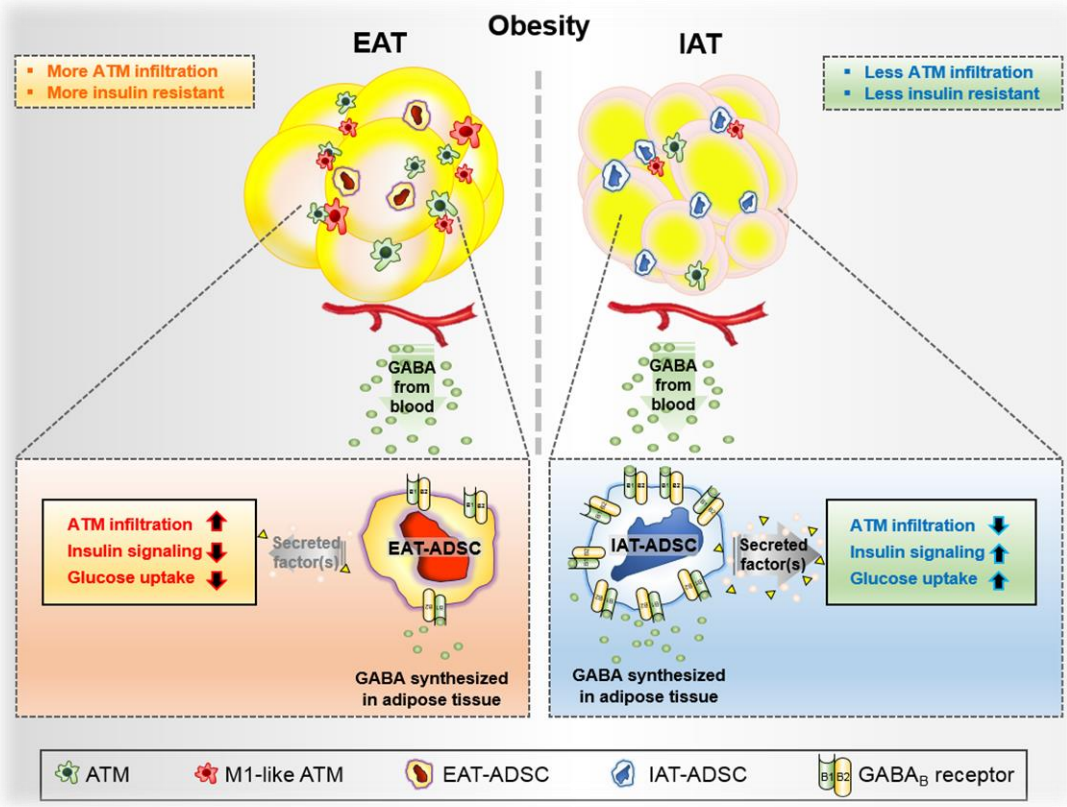

Fig. S9. A working model. In obesity, ADSC stimulated by GABA suppresses ATM infiltration selectively in IAT, but not in EAT.

Table S1. Serum metabolites comparisons between NCD and HFD fed mice

Compound Name	Relative Folds of Inductions (Average ± standard error, Log_2 scale, n = 3)		*p*-value (NCD vs HFD)
	NCD	HFD	
10-Hydroxydecanoic acid	-1.301	0.735±0.179063	0.00765
2-Aminobutyric acid	-1.102±0.342555	0.909±0.103344	0.020523
2-Hydroxybutyric acid	-1.074±0.246211	0.511±0.062588	0.018239
2-Oxobutyric acid	-1.277	0.339±0.096665	0.00356
2-Oxoglutaric acid	1.241±0.308649	-0.635±0.222267	0.010018
3-Hydroxy-3-methylglutaric acid	-1.304	0.731±0.143139	0.004911
3-Indoxylsulfuric acid	1.233±0.248622	-0.400±0.19012	0.007716
3-Ureidopropionic acid	-1.255	0.642±0.177242	0.008615
4-Methyl-2-oxovaleric acid 3-Methyl-2-oxovaleric acid	-1.168±0.054497	0.537±0.111277	0.000976
5-Aminovaleric acid	1.281±0.321594	-0.640	0.026904
Arg	1.073±0.507148	-0.367±0.201478	0.089629
Asn	-0.951±0.477486	1.066±0.055302	0.050031
Carboxymethyllysine	1.315±0.191113	-0.657	0.009258
Cholic acid	1.240±0.425	-0.620	0.048517
Creatine	1.166±0.451162	-0.500±0.132408	0.056357
Cystine	-1.106±0.500199	0.758±0.225108	0.047695
GABA	1.320±0.165462	-0.660	0.006915
Hippuric acid	1.311	-0.588±0.135389	0.000715
Imidazolelactic acid	-1.029±0.143103	0.517±0.114921	0.001327
Myristoleic acid	1.254±0.384909	-0.653±0.039178	0.037227
N^1-Methyl-4-pyridone-5-carboxamide	-1.005±0.215923	0.779±0.406116	0.029496
N^5-Ethylglutamine	1.328±0.086448	-0.704±0.02503	0.000875
N^6-Methyllysine	1.137±0.396193	-0.725±0.285309	0.022517
N-Acetylalanine	-1.048±0.156148	0.869±0.284556	0.008803
N-Acetylleucine	1.245±0.350648	-0.546±0.170946	0.02089
N-Acetyllysine	1.326±0.118029	-0.663	0.003501
Nicotinamide	1.109±0.197933	-0.334±0.096073	0.008064
Ophthalmic acid	1.244±0.414723	-0.622	0.045988
Perillic acid	-1.328	0687±0.044241	0.000482
Phenaceturic acid	-0.663	1.326±0.124414	0.003892
Phosphorylcholine	-1.164±0.120911	0.421±0.162235	0.001968
SDMA	-1.201±0.383463	0.800±0.197099	0.019046
S-Methylcysteine	-1.226±0.018734	0.703±0.259049	0.017151
Stachydrine	1.327±0.108758	-0.664	0.00297
Trigonelline	1.322±0.152799	-0.661	0.005888

Trimethylamine *N*-oxide	1.304±0.188833	-0.585±0.036175	0.008041
Trp	-1.005±0.303209	-0.585±0.036175	0.014791
Tyr	-0.831±0.314284	1.216±0.23614	0.007945
XA0027	1.250±0.260321	-0.782±0.032557	0.014889
β-Ala	1.227±0.332601	-0.473±0.151706	0.021858